R. & M. No. 3807

R. & M. No. 3807

PROCUREMENT EXECUTIVE, MINISTRY OF DEFENCE

AERONAUTICAL RESEARCH COUNCIL
REPORTS AND MEMORANDA

A 2D Partially-Parabolic Procedure for Axial-Flow Turbomachinery Cascades

By A. K. SINGHAL and D. BRIAN SPALDING

Mechanical Engineering Department, Imperial College

LONDON: HER MAJESTY'S STATIONERY OFFICE

1978

£4 net

A 2D Partially-Parabolic Procedure for Axial-Flow Turbomachinery Cascades

By A. K. SINGHAL and D. BRIAN SPALDING

Mechanical Engineering Department, Imperial College

Reports and Memoranda No. 3807*
October, 1976

Summary

A general finite-difference procedure is presented for the calculation of steady, two-dimensional 'partially-parabolic' flows, with special reference to turbine cascade problems. It can be used for incompressible, subsonic, supersonic or transonic flows. It can be characterised as an 'iterative space-marching' method.

The method is more economical in computer storage than time-marching procedures; and computer time is also low. The main distinguishing features of the method are:

(a) use of a streamline coordinate system,
(b) one-dimensional storage for all variables except pressure,
(c) solution by repeated marching integration from upstream to downstream.

The capabilities of the method are demonstrated by application to six different inviscid-flow problems. In each case, computed results are compared with the available analytical or experimental data. Good agreement is shown.

The method is capable of including momentum transfer across streamlines by viscous effects; it can easily incorporate a two-equation turbulence model; and heat transfer can be simultaneously calculated.

* Replaces A.R.C. 37 016

LIST OF CONTENTS

1. Introduction

1.1. The Problem Considered

The development of aerodynamically-efficient turbines and compressors requires the rapid and accurate prediction of flow in cascades of blades. In axial-flow machines, the blade-to-blade flow is often regarded as a two-dimensional one. Fig. 1 represents the flow geometry for a plane flow. The important features are:

(i) strong curvature in the flow passage;
(ii) circumferential periodicity of flow;
(iii) compressibility effects (subsonic, supersonic or transonic).

The present paper describes a numerical procedure for predicting flows which possess some or all of the above-mentioned features. The method can be easily extended to include other effects such as:

(a) rotation of blades;
(b) flow convergence resulting from variations of blade height or hub radius;
(c) friction;
(d) turbulence; and
(e) heat transfer.

1.2. Existing Methods

Numerous computational methods have been developed in the past for this problem; and Gostelow (1973)[4] has reviewed the capabilities and limitations of several of them. He pointed out that most of the methods were limited to subsonic flow; and the few methods which were applicable to transonic flows either required a priori knowledge of the sonic line in the flow, or were very expensive in computation time.

Most of the recent methods, e.g. McDonald (1971)[7], Gopalkrishnan and Bozzola (1971)[3], Denton (1975)[2], and Delaney and Kavanagh (1976)[1], are based on the 'time-marching' approach. This means that the steady-state solution is obtained by solving time-dependent, partial-differential equations. This practice has the merit of being easy to understand, but it possesses two inherent disadvantages:

(i) usually a great many time steps are required before a steady-state solution is reached, therefore, computations are expensive,
(ii) computer-storage requirements are also large because all the variables must be stored for the whole flow domain.

1.3. Main Features of the Present Method

The present method solves the *steady*-flow equations by a finite-difference technique and is very economical in computer storage and time requirements. It can be regarded as a combination of the Patankar–Spalding (1967)[9] procedure for predicting two-dimensional 'parabolic' flows, with the so-called 'semi-elliptic' (Spalding, 1971)[14] or 'partially-parabolic' method (Pratap and Spalding, 1975[11], 1976[12]) of handling 'elliptic' flow without flow reversal.

The novelties of the present method reside in the choices of:

(a) the coordinate system;
(b) the dependent variables; and
(c) the numerical solution scheme.

These will now be described.

(a) Coordinate System

A non-orthogonal coordinate system is employed in which the coordinate lines are:

(a) streamlines;
(b) a family of straight lines, parallel, in cascade problems, to lines through the leading edges of the blades.

A typical grid is shown in Fig. 2. The two independent variables are axial distance x, and stream function ψ. It should be pointed out here that the positions of streamlines in the x, y plane are not known in advance; instead, they are the outcome of computations. The main advantages of this coordinate system are as follows:

(i) Arbitrary-shaped boundaries, e.g. blade surfaces, can be handled very conveniently and accurately.
(ii) The governing flow equations are considerably simplified because the mass fluxes across the control-volume faces are known. For instance, in Fig. 3 the mass fluxes through faces 1 and 2 are equal to $\Delta\psi$; and mass fluxes through faces 3 and 4 are equal to zero.

(iii) The 'false viscosity' which afflicts numerical solution procedures in which streamlines cross grid lines obliquely is therefore absent.

(iv) Constant-x lines are particularly suitable for the imposition of the 'cyclic' boundary conditions outside the blade passage, according to which flow properties at either limit of the lines, although unknown, must be identical. They are also convenient for interpretation of the computed results.

(b) Dependent Variables

The following variables are treated as dependent variables, the values of which are to be found at all grid points:—

(i) streamwise-velocity, u;
(ii) y-direction component of velocity, v;
(iii) fluid pressure, p; and
(iv) fluid density, ρ.

It must be noted that the selected velocities are aligned with the coordinate lines, and thus are not orthogonal to each other. The advantage of this practice is that the momentum-conservation equation for each velocity contains only one pressure-gradient term, i.e. u depends on $\partial p/\partial s$ and v on $\partial p/\partial y$. The choice of velocity components has been the most critical factor in the success of the scheme.

(c) Numerical Solution Scheme

The method employs an iterative, forward-marching integration scheme which assumes the flow situation to be 'partially parabolic', Pratap and Spalding (1976)[12]. This means that downstream events are presumed to influence upstream ones only by way of pressure; for viscous effects in the upstream direction are negligible, at high Reynolds numbers; and recirculation (closed streamlines) is absent.

The distinctive features of the adopted procedure are:

(i) The pressure field is stored in a two-dimensional array.
(ii) Density, velocities and all other variables remain in one-dimensional storage, one x-location being treated at a time.
(iii) An iterative, marching-integration procedure is adopted, whereby several sweeps of the flow domain are made; in each sweep a better estimate of the pressure field is obtained.

Further details of the calculation steps are given in Section 2.4.

It can be noted from the above description that the computer-storage requirements are minimal. The saving, as compared with time-marching methods, becomes even more significant when additional dependent variables such as turbulence kinetic energy, stagnation enthalpy, etc., are also to be solved.

1.4. Outline of the Paper

The remainder of the paper is divided into three sections. Section 2 describes the governing flow equations, some important auxiliary relations, the boundary conditions, and the main steps of the solution procedure. Section 3 presents computed results for six test cases, comprising one incompressible, one subsonic and four transonic problems. In each case, the computed solution is compared with the available analytical or experimental data. Concluding remarks are made in Section 4.

2. The Solution Procedure

2.1. Governing Equations

For a plane, two-dimensional, inviscid, compressible flow, the governing equations are written as follows:
Streamwise momentum-conservation equation:

$$u_2^2 - u_1^2 = \frac{2\gamma}{\gamma - 1}\left(\frac{p_1}{\rho_1} - \frac{p_2}{\rho_2}\right); \tag{1}$$

y-direction momentum-conservation equation:

$$\Delta\psi(v_2 - v_1) = (p_3 - p_4)\,.\,\Delta x; \tag{2}$$

Equation for kinematic compatibility of flow:

$$\Delta y_2 - \Delta y_1 = \Delta x(\tan\alpha_4 - \tan\alpha_3); \tag{3}$$

Equation of state:

$$\rho = \rho_0 \left(\frac{p}{p_0}\right)^{1/\gamma}. \tag{4}$$

The meanings of the symbols are explained in the List of Symbols. Suffixes 1, 2, 3 and 4 refer to the average values pertaining to the respective faces of the control volume of Fig. 3. Suffix 0 denotes the stagnation condition.

Some remarks on equations

Equation (1) is a form of the Bernoulli's equation for compressible flow (Liepmann and Roshko, 1966)[6]. It can also be regarded as a 'total energy' equation; however, its main function is to relate the streamwise velocity, u, to the pressure. Equation (2) has been obtained by applying the momentum-conservation law to the control volume of Fig. 3.

Equation (3) is a geometrical relation; it is the counterpart of the continuity equation of a fixed-grid coordinate system. In equation (3), Δy and α are auxiliary quantities, which are calculated from primary variables, as explained in Section 2.2.3.

Equation (4), like equation (1), is valid for isentropic flow; more general relations can be incorporated, if desired.

2.2. Some Important Details

2.2.1. Staggered-Grid Practice

The velocity components and pressure are stored in the 'staggered' positions on the finite-difference grid. The boundaries of the various control volumes, and the storage locations of variables, are shown in Fig. 4.

2.2.2. Upwind-differencing Practice

Upwind differences of momentum fluxes are used in the momentum-conservation equations. The final forms of these equations, as employed in the method, are:

$$u_e^2 - u_w^2 = \frac{2\gamma}{\gamma - 1}\left(\frac{p_P}{\rho_P} - \frac{p_E}{\rho_E}\right), \tag{5}$$

$$\Delta\psi(v_n - v_{nw}) = (p_P - p_N)\,.\,\Delta x. \tag{6}$$

2.2.3. Calculation of Auxiliary Quantities

As mentioned in Section 2.1, α and Δy are calculated from the primary variables; the relationships used are:

$$\text{Kinematics of flow:} \quad \alpha = \sin^{-1}\frac{v}{u}, \tag{7}$$

$$\text{Continuity:} \quad \Delta y = \frac{\Delta\psi}{\rho u \cos\alpha}. \tag{8}$$

In equation (7), v and u are velocities interpolated for the point at which α is to be calculated. In equation (8), the term $\rho u \cos\alpha$ should be evaluated at the centre of the control-volume face for which Δy is to be calculated.

2.2.4. A Pressure-correction Equation

In accordance with the requirements of the SIMPLE (Semi-Implicit Method for Pressure-Linked Equations) algorithm of Patankar and Spalding (1972)[10], a pressure-correction equation is derived. Full details of the derivation are given in a separate report by Singhal (1977)[13]; and the main steps are explained in the appendix of this report. Here, only the final form is presented. It is, with reference to Fig. 5:

$$(A_N + A_S + A_E + A_W)p'_P = A_N p'_N + A_S p'_S + \varepsilon_P. \tag{9}$$

The A coefficients contain mass fluxes, areas and inclinations of control-volume faces. The ε_P term expresses the kinematic-compatibility error, for grid node P, as calculated below:

$$\varepsilon_P \equiv (\Delta y_e^* - \Delta y_w^*) - \Delta x \, (\tan \alpha_n^* - \tan \alpha_S^*). \tag{10}$$

Superscript *, given to Δy and α, denotes that these quantities are based on an estimated pressure field. The purpose of the pressure-correction equation is to correct the pressure and velocity fields so as to annihilate the error, ε, at all grid locations in the flow domain.

2.2.5. Treatment of Compressibility

Irrespective of whether the flow is subsonic or supersonic, the equations (4), (5), (6) and (9) are solved, at each grid node, in an identical manner. However, the elliptic and hyperbolic behaviours of the subsonic and supersonic regions are expressed through the differing ways of computing the mass velocity (ρu). This quantity ρu is used in equation (8) for calculating the cell-face height Δy.

For this purpose, a 'convective-velocity' practice (Spalding, 1976)[15], has been adopted. According to this practice, ρu at a typical location, point e in Fig. 5, is calculated as follows:

$$(\rho u)_e = \rho_P \cdot u_{\text{convective}}, \tag{11}$$

where for subsonic flow,

$$u_{\text{convective}} \equiv u_e \cdot \left(\frac{p_E}{p_P}\right)^{1/\gamma},$$

and for supersonic flow, $u_{\text{convective}} = u_w$.

For an isentropic flow, the above prescription can also be interpreted as:

$$(\rho u)_e = \rho_E u_e \quad \text{for subsonic flow}$$

and

$$(\rho u)_e = \rho_P u_w \quad \text{for supersonic flow.}$$

The main implications of this practice are:

(i) In a supersonic region, $(\rho u)_e$ is independent of the downstream pressure p_E. This enforces the principle that influences cannot travel upstream in supersonic flow.

(ii) In the flow regions where Mach numbers are close to or greater than unity, the large density changes provoke no numerical instability; for, in the product $\rho_P u_w$ or $\rho_E u_e$, velocity is considered at an upstream point relative to the location of density; and therefore, for a pressure change at the location of density, the considered ρ and u always vary in the opposite directions.

It should be remarked that this deliberate contrivance of features in the finite-difference equations which conform to known features of real flows is both necessary and proper. Finite-differencing 'losses' information which the differential equations possess; and sometimes this 'loss' must be artificially made good.

2.3. Boundary Conditions

At the boundaries of the solution domain (Fig. 1), the flow conditions are specified in the following manner.

Inlet plane: Stagnation pressure and density, and flow direction, are specified.
Outlet plane: Static pressure is specified.

In some cases, where the exit flow condition is subsonic, static pressure can also be prescribed at the inlet plane instead of at the exit plane. In these circumstances, the exit static pressure is an outcome of the solution, and the boundary condition for the outlet plane can be changed to one of the following two types:

(i) cross-stream variation of pressure is specified; or
(ii) streamwise derivative of pressure is specified.

Solid boundaries: Local surface inclinations, with reference to the x-direction, are specified.

Dividing streamline boundaries, upstream and downstream of the cascade.

These are treated in the same way as solid boundaries, except that their local inclinations are calculated, as explained below, from the periodicity ('cyclic boundary') conditions.

Fig. 6 shows a typical arrangement of streamlines in the cyclic-boundary region. The bounding streamlines are numbered as 1 and n. The line $2'$ is a pseudo streamline which is parallel to streamline 2 and displaced from it by a distance equal to pitch. Periodicity of flow implies that the flow properties are identical at corresponding points such as A and A', B and B', D and D', etc.

In order to determine the inclination α_B, the velocity v_B is calculated by applying Equation (6) to the control volume, shown by the shaded area in Fig. 6; and the value of streamwise velocity u_B is interpolated from the u-velocities of the adjoining points, viz. C, D, E and F. Then α_B is simply calculated from Equation (7).

Near-round-edge regions

At present, the regions close to the round edges of the blades are treated in an approximate manner, i.e. by placing small 'cusps' at the round edges. At the leading edge, a cusp is made symmetrical to the inlet flow direction, while a trailing-edge cusp satisfies the Kutta–Joukowski condition of zero load.

These 'cusps' are no more than aids to thought and verbal description, expressing the fact that, in the vicinity of the leading and trailing edges, large changes of blade-surface angle occur over distances which are of the same order as the grid size. More sophisticated practices are in the course of development.

2.4. Sequence of Calculation Steps

The main features of the numerical-solution scheme were outlined in Section 1.3. In this section, the detailed calculation steps are summarised as follows:

(1) The pressure field is first assigned guessed values. For example, the pressure may be assumed to be uniform in the y-direction and to vary linearly in the axial direction.

(2) Inlet distributions of u and ρ are obtained, from isentropic-flow relations, from the static pressure, the stagnation pressure and the density. v is deduced from u and the given α.

(3) At the next downstream section, u, v and ρ are calculated, by solving equations (4), (5) and (6).

(4) From the just-computed velocities and densities, the kinematic-compatibility errors and other coefficients of the pressure-correction equations are calculated. A set of pressure-correction equations, one equation for each grid node of the section under consideration, is obtained. These are solved simultaneously by applying the tri-diagonal matrix algorithm (TDMA) along the line of constant x.

(5) The corresponding corrections are now applied to the pressures, velocities and densities of the current-plane nodes.

(6) In addition to the above-mentioned *local* pressure corrections, average-pressure adjustments are also made so as to ensure that the calculated overall width of flow, in the y-direction, is exactly equal to the actual dimension.

(7) The next downstream section is chosen; and steps 3 to 6 are repeated. This stepwise march is continued until the end of the flow domain is reached. This completes one marching sweep; and a new, improved, two-dimensional distribution of pressure has been obtained.

(8) Steps 2 to 7 are repeated until the pressure corrections or the kinematic-compatibility errors have become smaller than a pre-assigned value. On the last sweep, the converged distributions of velocities, pressure and other quantities of interest are printed out.

3. Applications

In this section, the capabilities of the solution procedure, described in Section 2, are demonstrated by way of six examples. For each example, the description is divided into two parts, viz. (i) statement of problem, and (ii) presentation of computed results and their comparison with available analytical or experimental results. Computational details of all the examples are summarised in a table at the end of this chapter.

3.1. Example 1: Incompressible Flow past a Cylinder placed in a Channel

In order to test the basic solution scheme, an inviscid, incompressible flow, without any cyclic boundaries, has been selected as the first example. Fig. 7 shows the flow geometry, together with the selected domain of integration and a typical grid arrangement.

An exact analytical solution can be obtained by considering an infinite series of doublets placed at the y-axis, at equal intervals (Ex. 39, p. 229, Milne-Thompson (1962)[8]. The resultant stream function is:

$$\psi = U_\infty y - U_\infty \cdot \frac{\pi}{4} \cdot \frac{\sin(\pi/2 \cdot y)}{\cosh[(\pi/2)x] - \cos[(\pi/2)y]}. \tag{12}$$

The streamline $\psi = 0$ includes the x-axis and the contour of the cylinder.

For numerical computations, the coordinates of the cylinder surface were specified. In addition, the following conditions were supplied as boundary conditions:

(i) uniform inlet velocity;

(ii) zero streamwise gradient of pressure at the exit plane.

Fig. 8 shows the comparison between the predicted and analytically-solved streamlines; the agreement is very satisfactory.

3.2. Example 2: Subsonic Flow in a NASA Turbine Stator Cascade

In this example, a two-dimensional, compressible flow is considered in a cascade in which flow remains subsonic throughout. The selected problem is flow at the mean-diameter section of a stator of a NASA turbine, operating at the design mass flow rate; relevant experimental data have been reported by Whitney et al (1967)[16]. The cascade has round-edged blades.

For computations, in order to avoid discontinuities in the grid, small cusps have been placed at the leading and trailing edges of the blades.

The predicted and experimental distributions of surface Mach number are compared in Fig. 9. The computed Mach numbers agree well with the experimental data.

3.3. Example 3: Transonic Flow in Hobson's First Impulse Cascade

This example considers the first of the two impulse cascades, for which analytical solutions, obtained by the Hodograph method, are reported by Hobson (1974).

In this problem, flow is subsonic at both inlet and outlet sections; and there is an embedded supersonic region near the centre of the suction surface. Flow is expected to be free of shocks.

Results

Figs. 10 and 11 show the computed streamlines and contours of critical Mach number ($M^* = u/u^*$). It may be observed that the computed flow field is fairly symmetrical.

In Fig. 12, the computed distributions of surface velocities are compared with the Hodograph design data; the agreement is quite good except at the central part of the suction surface, where the predicted velocities are relatively low. No reason is apparent for this discrepancy. However, it may be pointed out here that in a Hodograph method an inverse problem is solved, i.e. blade shape is calculated, by a finite-difference technique, for the pre-selected velocity distribution as a function of flow direction; this calculation is no less subject to truncation errors than the present one.

Solutions of other methods, presented at a NATO conference at Cambridge University in 1973, also showed some discrepancies in this region; these solutions are reported in Hobson's Ph.D. thesis[5].

3.4. Example 4: Transonic Flow in Hobson's Second Impulse Cascade

This case is very similar to that of example 3; but the impulse blades are relatively of thinner section, and the expected supersonic region is smaller.

Fig. 13 demonstrates that the present predictions agree well with the Hodograph design.

3.5. Example 5: Transonic Flow in a VKI Gas Turbine Cascade

This example considers a cascade flow which is subsonic at inlet and supersonic at outlet. Problem specifications, experimental measurements and theoretical predictions of several other methods are reported in the VKI Lecture Series 59 (1973).

Computed results

Computations have been made for two different flow conditions, specified by the outlet Mach numbers which are: (i) 1·31 and (ii) 1·11. Figs. 14 and 15 present the calculated Mach-number contours in the flow field. From these two figures, it can be seen that in the downstream part of the flow domain there are

noticeably different shock structures; but, in the upstream region, changes in Mach numbers are insignificant.

Figs. 16 and 17 compare the predicted and experimental values of surface Mach numbers for the two flow conditions considered. The agreement of the present method with experiments is excellent except that, in Fig. 17, slight discrepancies appear on the suction surface near to the trailing edge. These discrepancies may be ascribed to one or both of the following:

(i) Neglect of viscous effects: These are most significant in the rear part of the suction surface where adverse pressure gradient exists; thus the boundary layer can grow and the shock boundary-layer interactions can change the flow significantly.

(ii) Limited accuracy of the finite-difference procedure near the round edges of blades.

It may also be pointed out here that none of the other methods, reported in VKI Lecture Series, were able adequately to predict the steep variations of Mach number near the trailing edges of this cascade.

3.6. Example 6: Transonic Flow in a VKI Steam Turbine Cascade

This is the second test case of VKI Lecture Series 59 (1973). It presents a very severe test of any finite-difference scheme since extremely steep gradients of flow properties occur in both pitchwise and streamwise directions. Fig. 18 illustrates the cascade geometry; pitchwise grid lines are also shown to give an idea of the axial grid spacings used in the present computations. The computed streamlines and Mach-number contours are exhibited in Figs. 19 and 20.

Fig. 21 shows the comparison of predicted and experimental surface-Mach-numbers. Once again, agreement between the computed results and experimental data is good over most of the blade surface.

3.7. Computational Details

Computations were carried out on the CDC 6600 computer of London University. Execution time requirements of the examples described in Sections 3.1 to 3.6 are indicated in the following table:

Example No.	Identification	Grid size $N_y \times N_x$	Execution time on CDC 6600 computer (seconds)
1	The cylinder problem	11×25	7
2	NASA stator cascade	8×27	9
3	Hobson's first cascade	11×30	15
4	Hobson's second cascade	8×30	10
5	VKI gas turbine cascade	10×30	20
6	VKI steam turbine cascade	20×38	52

It was established, by variations of the grid fineness and by increasing the number of iterations that the physically-significant results of the computations were substantially independent of these factors.

4. Concluding Remarks

(i) The present paper has described a simple and economical solution procedure for calculating two-dimensional, partially-parabolic flows, such as flow in turbine cascades. The presented examples have illustrated its capability of solving incompressible, subsonic and transonic flow problems.

(ii) The main merits of the method derive from its use of (a) the non-orthogonal streamline coordinate system, (b) the velocity components which are aligned with the local coordinate directions, and (c) the use of one-dimensional storage for all variables except pressure.

(iii) Further developments of the method, now in progress, include:

(a) Inclusion of physical effects such as friction, turbulence, heat transfer, rotation of blades, and convergence of flow resulting from hub-radius and blade-height changes.

(b) Calculations of two-dimensional through-flow, in turbomachines, by neglecting circumferential variations, in the meridional plane.
(c) Allowance for 'doubling back' of streamlines.
(d) Applications to external flows.

5. Acknowledgements

The authors wish to acknowledge many helpful discussions with Drs. D. G. Tatchell and A. Thyagaraja. One of the authors (A. K. Singhal) was supported during the course of this research by a scholarship from CHAM Limited. The computer code employed is a version of the PHOENICS 2/PP/PSI code, on loan from CHAM.

The authors also with to thank Mrs. Christine MacKenzie for preparing the typescript.

LIST OF SYMBOLS

A	Coefficient in the pressure-correction equation.
M	Mach number.
p	Fluid pressure.
s	Distance along a streamline.
u	Stream-wise velocity or total velocity.
v	y-direction component of velocity.
x	Reference direction, e.g. direction of turbine axis.
y	Direction normal to x.

Greek

α	Local streamline inclination with reference to the x-direction.
γ	Ratio of specific heats.
ε	Kinematic-compatibility error.
ψ	Stream function.
ρ	Fluid density.

Subscripts

N, S, E, W	Refer to the neighbouring grid nodes located in north, south, east and west directions, respectively.
n, s, e, w	Refer to the mid-node locations.
P	A typical grid node.
0	Refers to the fluid stagnation conditions.
1, 2, 3, 4	Refer to control-volume faces, Fig. 3.

Superscripts

$'$	Denotes correction component.
$*$	Refers to fluid properties based on approximate pressure field; also used to denote critical (or sonic) condition.

REFERENCES

No.	Author(s)	Title
1	R. A. Delaney and P. Kavanagh ...	Transonic flow analysis in axial-flow turbo-machinery cascades by a time-dependent method of characteristics. *J. Engg. Power*, Trans. ASME, Series A, Vol. 98, pp. 356–364 (1976).
2	J. D. Denton	A time-marching method for two and three-dimensional blade to blade flows. Central Electricity Generating Board, Research Dept. R/M/R215 (January 1975).
3	S. Gopalkrishnan and R. Bozzola ..	A numerical technique for the calculation of transonic flows in turbomachinery. ASME Paper 71-GT-42 (1971).
4	J. P. Gostelow	Review of compressible flow theories for airfoil cascades. *J. Engg. Power*, Trans. ASME, Series A, Vol. 95, no. 4, pp. 281–292 (1973).
5	D. Hobson	Shock-free transonic flow in turbomachinery cascades. Ph.D. Thesis, Cambridge University, UK (September 1974).
6	H. W. Liepmann and A. Roshko ...	*Elements of gas dynamics.* John Wiley Inc., (1966).
7	P. W. McDonald	The computation of transonic flow through two-dimensional gas-turbine cascades. ASME Paper 71-GT-89 (1974).
8	L. M. Milne-Thompson	*Theoretical hydrodynamics.* MacMillan & Co., 4th Edition (1962).
9	S. V. Patankar and D. B. Spalding .	A finite-difference procedure for solving the equations of the two-dimensional boundary layer. *Int. J. Heat Mass Transfer*, Vol. 10, pp. 1389–1412 (1967).
10	S. V. Patankar and D. B. Spalding .	A calculation procedure for heat, mass and momentum transfer in three-dimensional parabolic flows. *Int. J. Heat Mass Transfer*, Vol. 15, pp. 1787–1806 (1972).
11	V. S. Pratap and D. B. Spalding ...	Numerical computations of flow in curved ducts. *Aeronautical Quarterly*, Vol. 26, pp. 219–228 (1975).
12	V. S. Pratap and D. B. Spalding ...	Fluid flow and heat transfer in three-dimensional duct flows. *Int. J. Heat Mass Transfer*, Vol. 19, pp. 1183–1188 (1976).
13	A. K. Singhal	Flow in axial turbomachinery cascades. Ph.D. Thesis, to be submitted to London University (1977).
14	D. B. Spalding	Unpublished notes at Imperial College, London, Mechanical Engineering Department (1971).
15	D. B. Spalding	Unpublished notes at Imperial College, London, Mechanical Engineering Department (1976).

No.	*Author(s)*	*Title*
16	W. T. Whitney, E. M. Szanca, T. P. Moffit and D. E. Monroe	Cold-air investigation of a turbine for high-temperature-engine application. NASA TN D-3751 (1967).

APPENDIX

Derivation of the Pressure-Correction Equation

The basic idea of the SIMPLE algorithm is: first, to solve the momentum-conservation equations, using approximate values of pressures; and, then, to correct the pressures and velocities so that the continuity, or in the present case, kinematic-compatibility, requirement is satisfied at each grid node. These corrections are applied for *one* cross-stream section at a time, and are calculated as follows:

(a) The pressure and velocity fields are expressed as:

$$p = p^* + p', \tag{A-1}$$

$$u = u^* + u', \tag{A-2}$$

$$v = v^* + v', \tag{A-3}$$

where the primed quantities represent the corrections to the approximate (starred) values.

Similarly, the auxiliary quantities can be expressed as:

$$\rho = \rho^* + \rho'; \tag{A-4}$$

$$\Delta y = \Delta y^* + \Delta y', \tag{A-5}$$

$$\alpha = \alpha^* + \alpha'. \tag{A-6}$$

(b) Application of the kinematic-compatibility condition (Equation 3) to the control volume of Fig. 5 yields:

$$\Delta y_e - \Delta y_w = \Delta x(\tan \alpha_n - \tan \alpha_s), \tag{A-7}$$

But ε_P, the kinematic-compatibility error in the region surrounding grid node P, is defined (see Section 2.2.4) by:

$$\Delta y_e^* - \Delta y_w^* \equiv \Delta x[(\tan \alpha_n)^* - (\tan \alpha_s)^*] + \varepsilon_P. \tag{A-8}$$

Subtracting (A-8) from (A-7) yields:

$$\Delta y_e' - \Delta y_w' = \Delta x[(\tan \alpha_n)' - (\tan \alpha_s)'] - \varepsilon_P. \tag{A-9}$$

(c) Next, the quantities $\Delta y'$ and $(\tan \alpha)'$ are expressed in terms of u', v' and ρ'.

For example, by differentiating equation (8), there results:

$$\frac{\Delta y'}{\Delta y} = -\left[\frac{\rho'}{\rho} + \frac{u'}{u} + \frac{(\cos \alpha)'}{\cos \alpha}\right]. \tag{A-10}$$

Further, $\cos \alpha$ and $\cos \alpha'$ are also expressed in terms of the velocity components as follows:

$$\cos \alpha = \frac{\sqrt{u^2 - v^2}}{u}; \tag{A-11}$$

$$(\cos \alpha)' = \frac{\partial(\cos \alpha)}{\partial u} u' + \frac{\partial(\cos \alpha)}{\partial v} v'. \tag{A-12}$$

Similarly, $\tan \alpha$ and $(\tan \alpha)'$ can be related to velocity components.

(d) Now, u', v' and ρ' are related to the pressure corrections at the adjoining grid nodes by relations such as:

$$v_n' = \frac{\Delta x}{\Delta \psi} \cdot (p_P' - p_N'), \tag{A-13}$$

$$u'_e = \frac{1}{(\rho u)_e} \cdot (p'_P - p'_E), \tag{A-14}$$

$$\rho'_P = \left(\frac{\rho}{\gamma p}\right)_P. \tag{A-15}$$

These equations can be derived by substituting equations (A-2), (A-1) and (A-3) into equations 2, 1 and 4 respectively.

(e) The relations expressed above are then substituted into equation (A-9); the coefficients for p'_P are collected and rearranged to obtain the form which appeared in Section 2.2.4, as equation (9):

$$(A_N + A_S + A_E + A_W)p'_P = A_N p'_N + A_S p'_S + \varepsilon_P. \tag{A-16}$$

It may be noted that in equation (A-16), pressure corrections of the upstream and downstream nodes, p'_E and p'_W, do not appear. The reason is that corrections are not being made on the constant-x lines containing E and W at the time in the computation at which P, N and S are being attended to. Of course, in the repeated-space-marching procedure, all corrections are made, and all kinematic-compatibility errors reduced to acceptably small sizes, before the end.

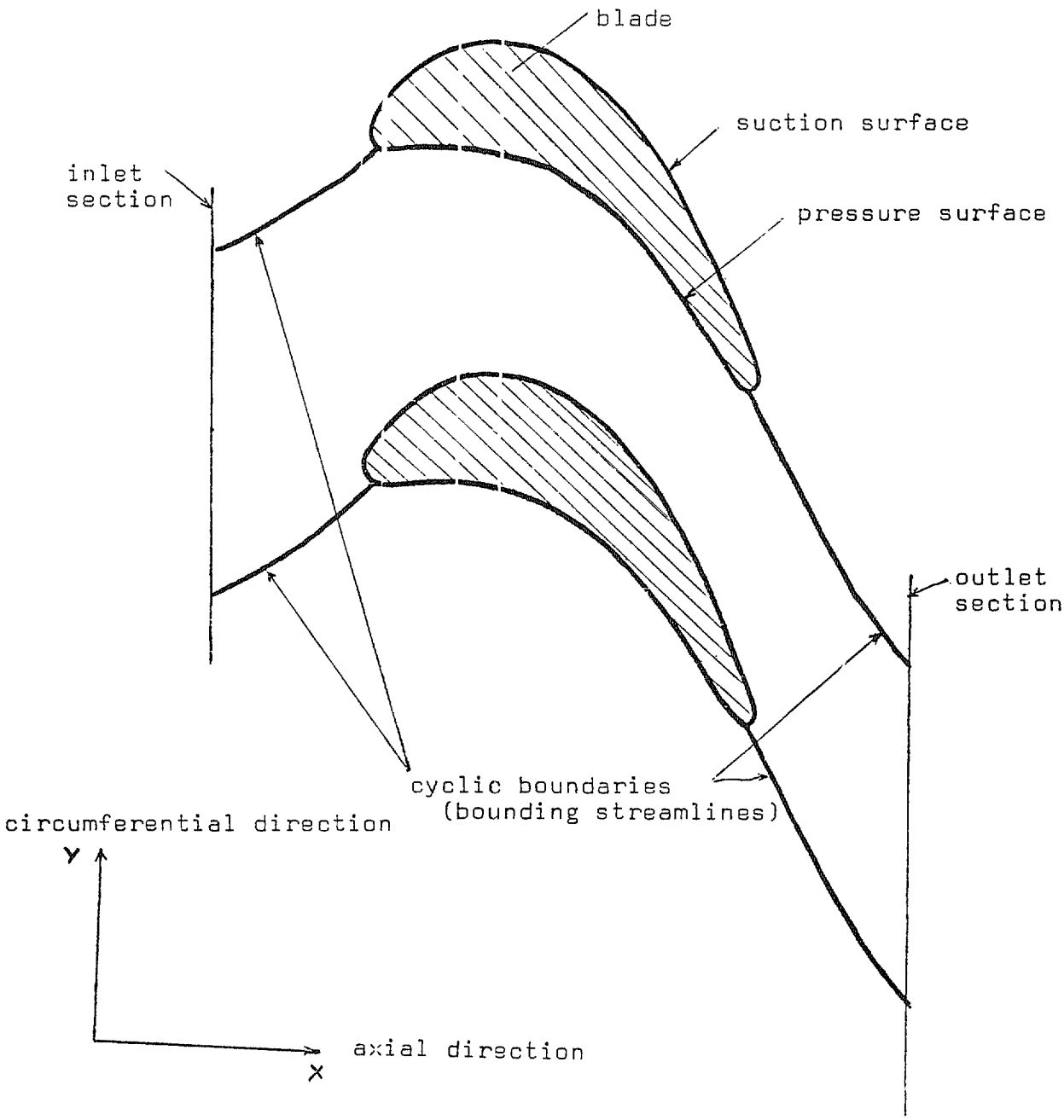

FIG. 1. The flow geometry.

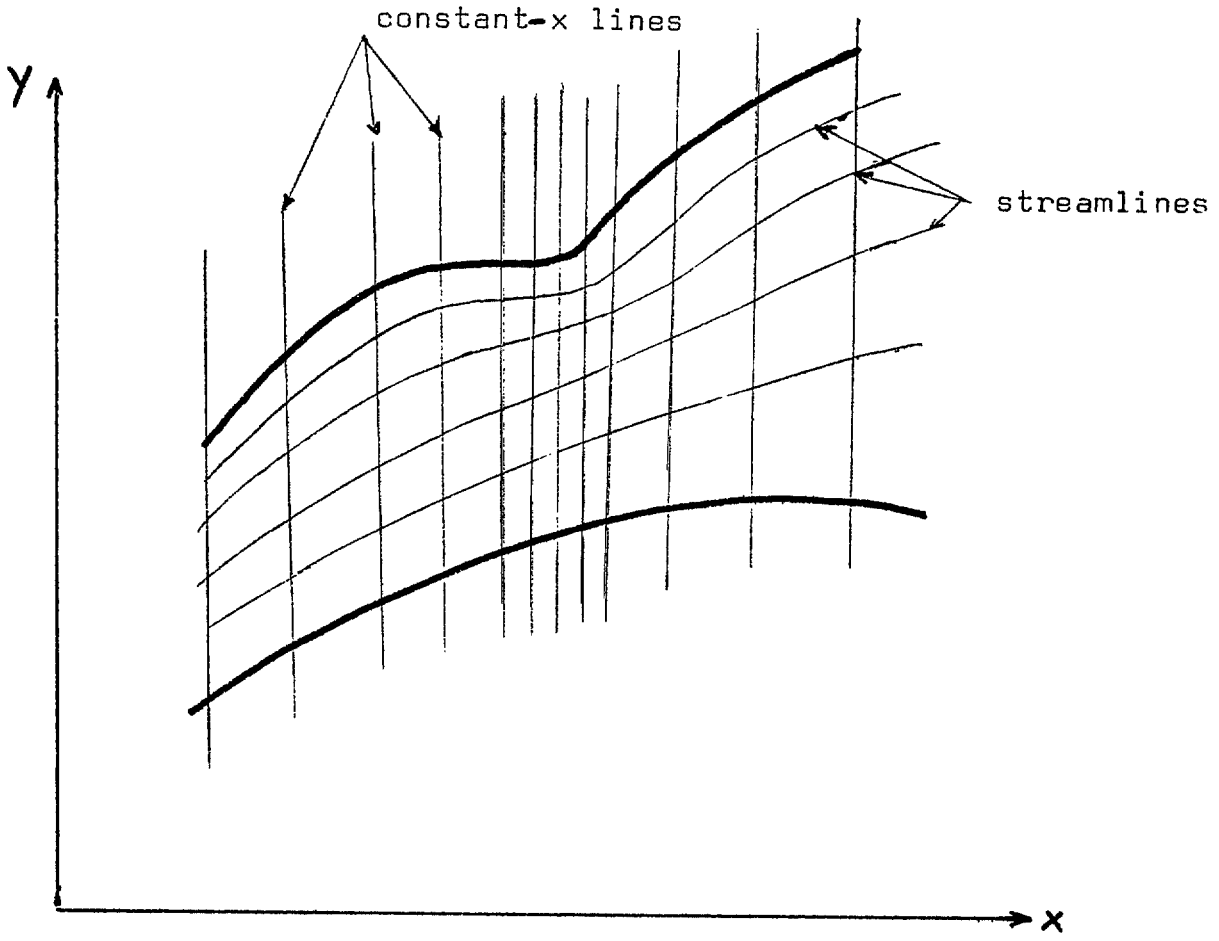

FIG. 2. The non-orthogonal grid.

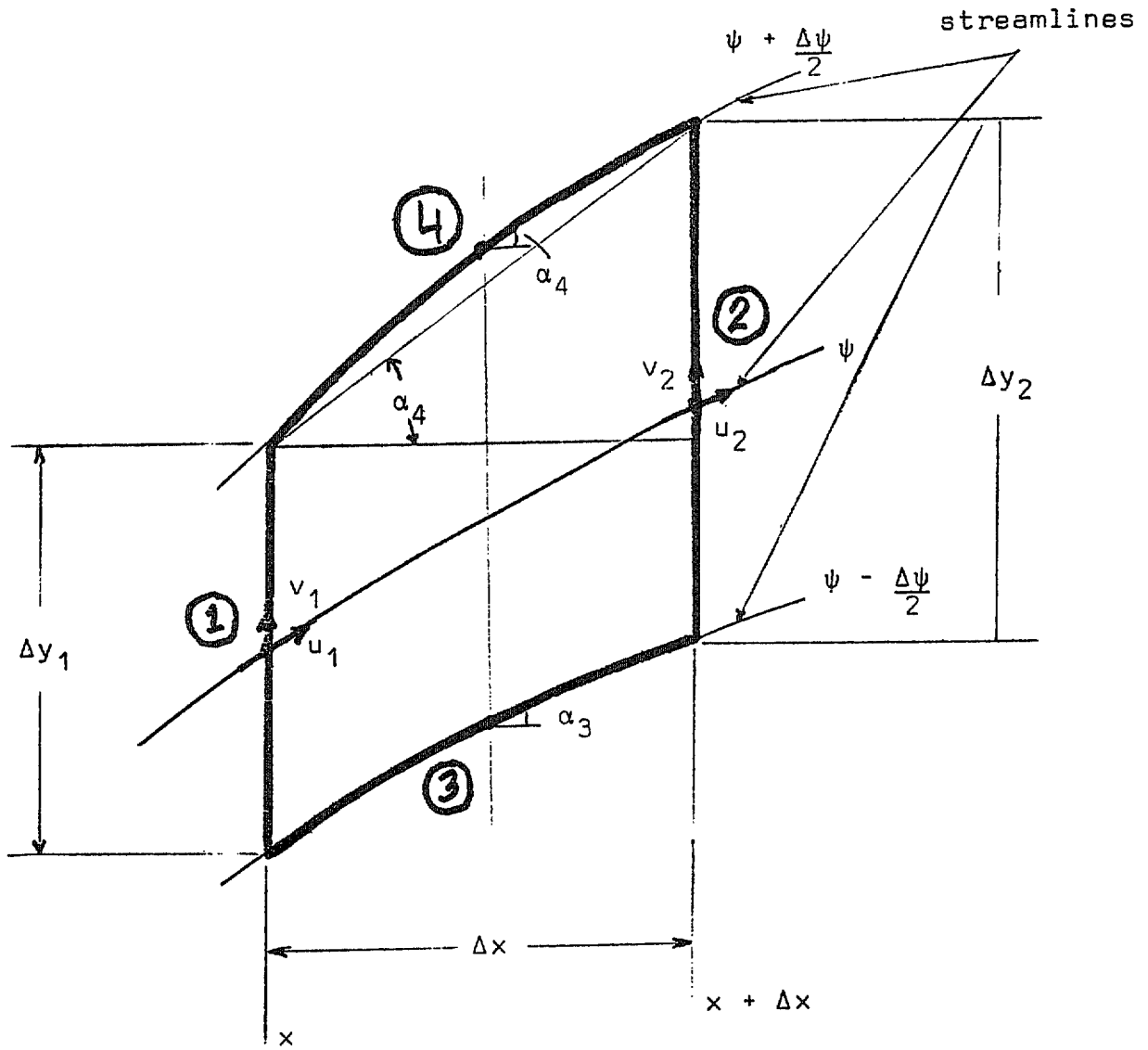

FIG. 3. A typical control volume.

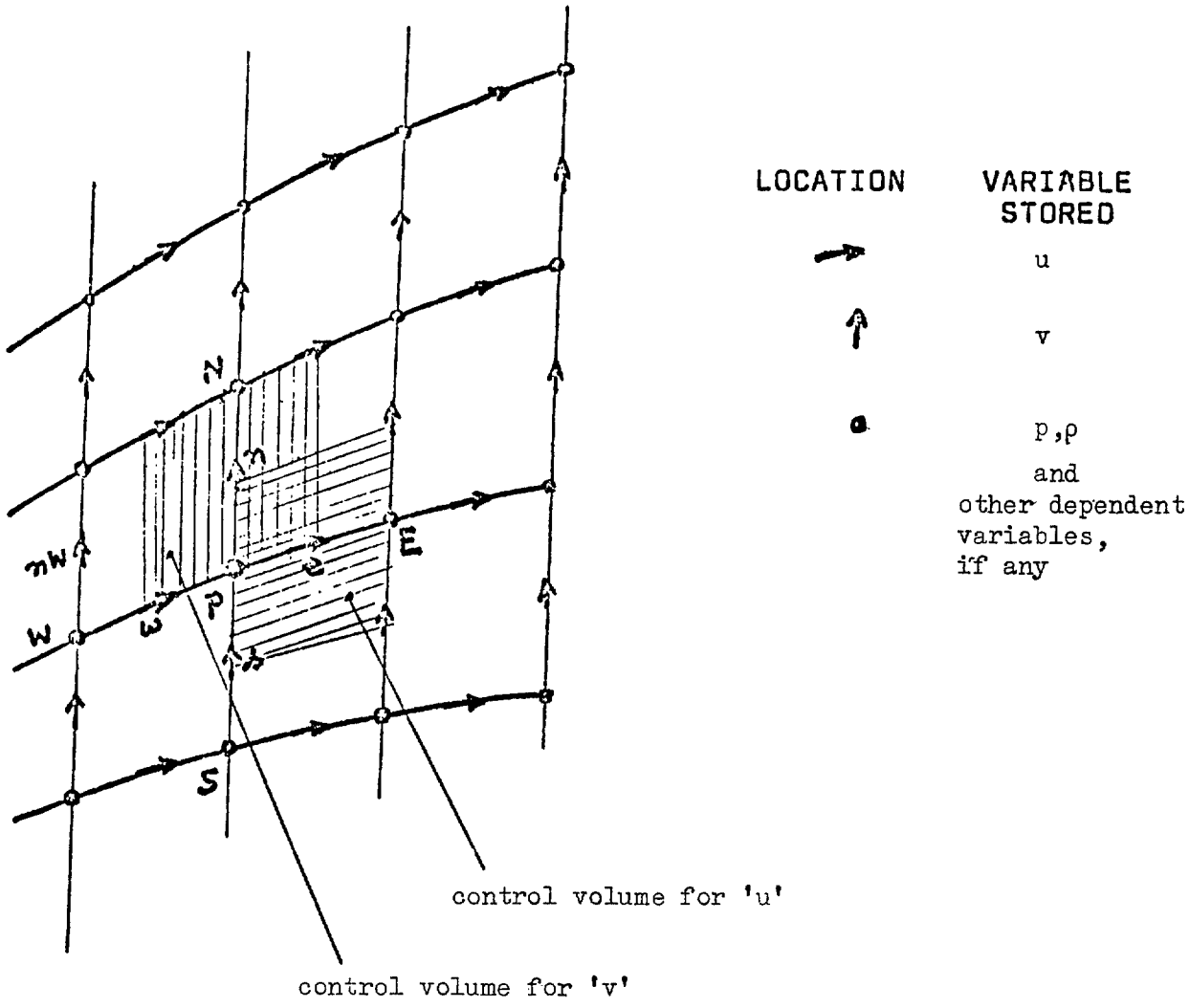

FIG. 4. The staggered-grid arrangement.

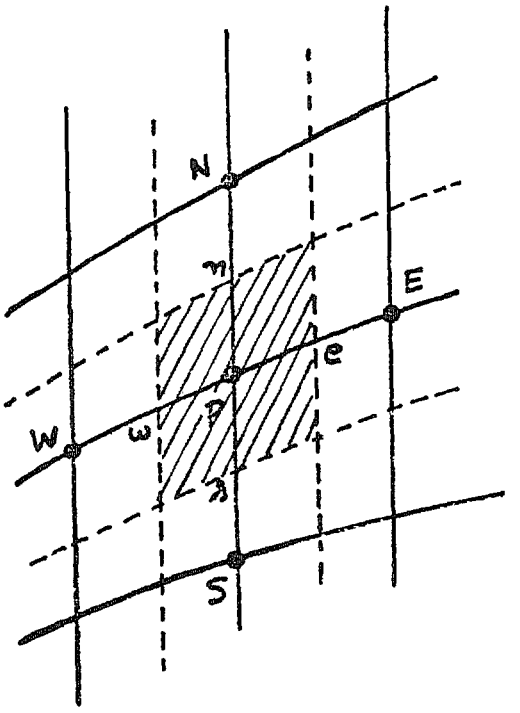

FIG. 5. Control volume used in derivation of pressure-correction equation for grid node *P*.

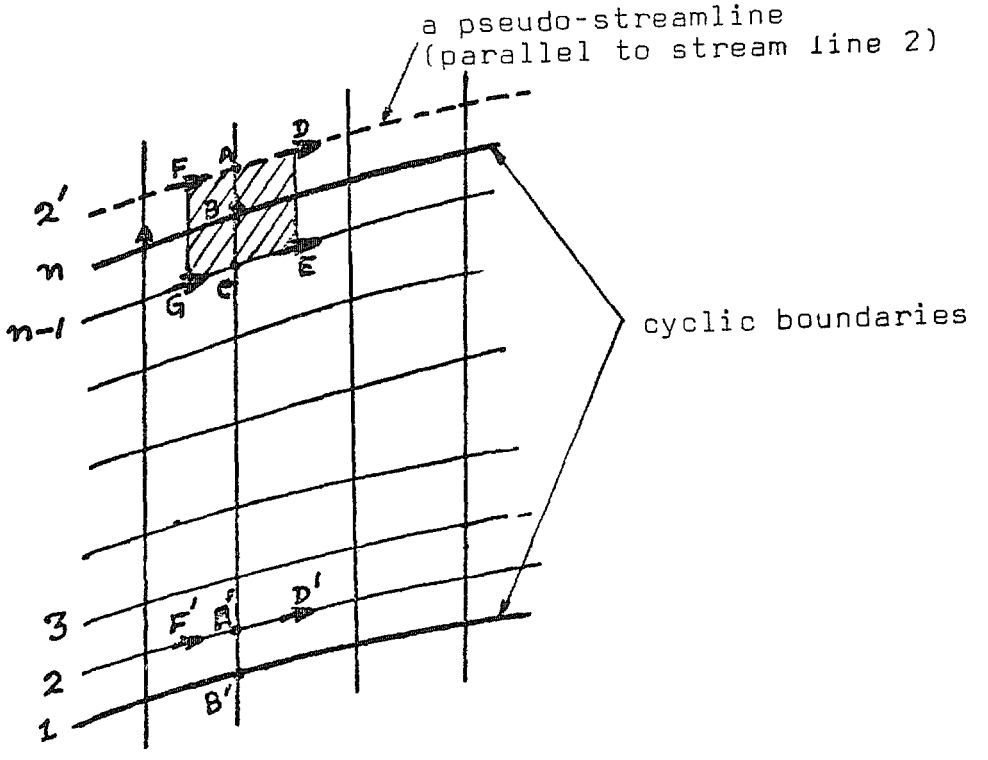

FIG. 6. Streamlines in the cyclic-boundary region.

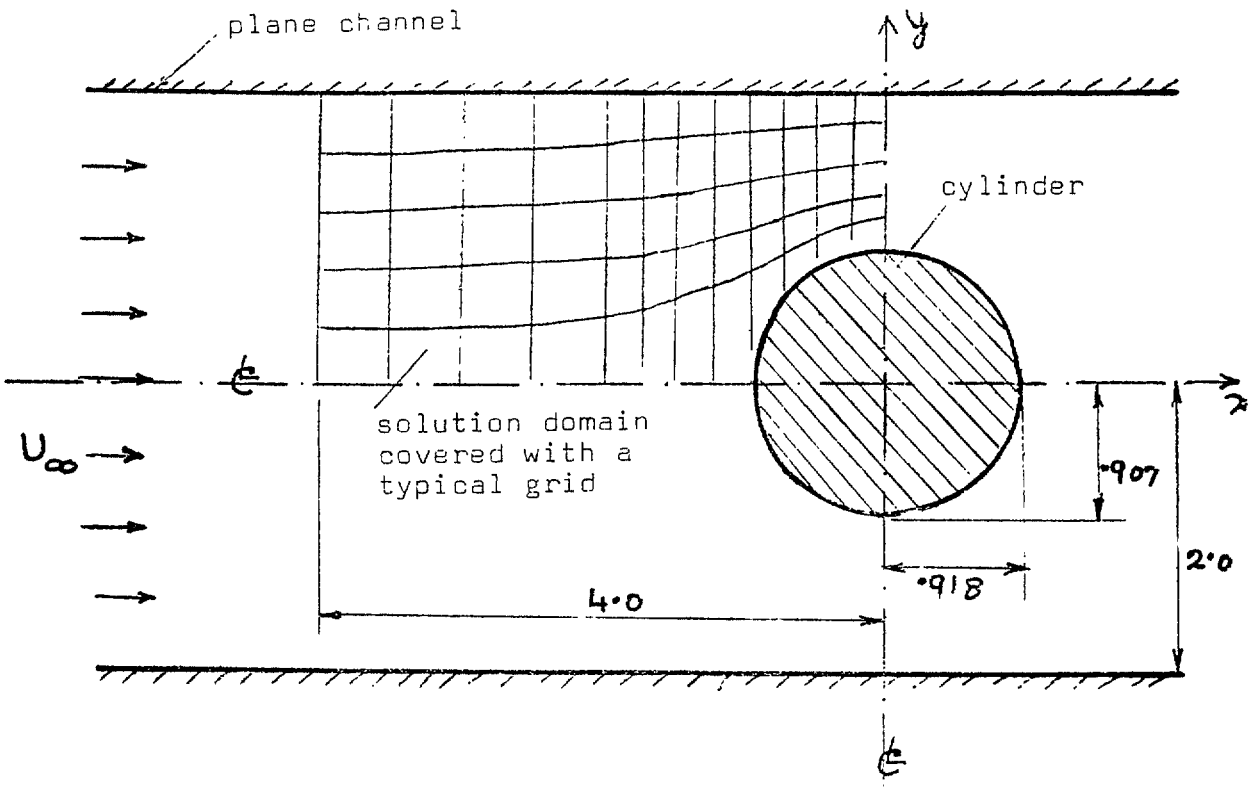

FIG. 7. Flow geometry of example 1.

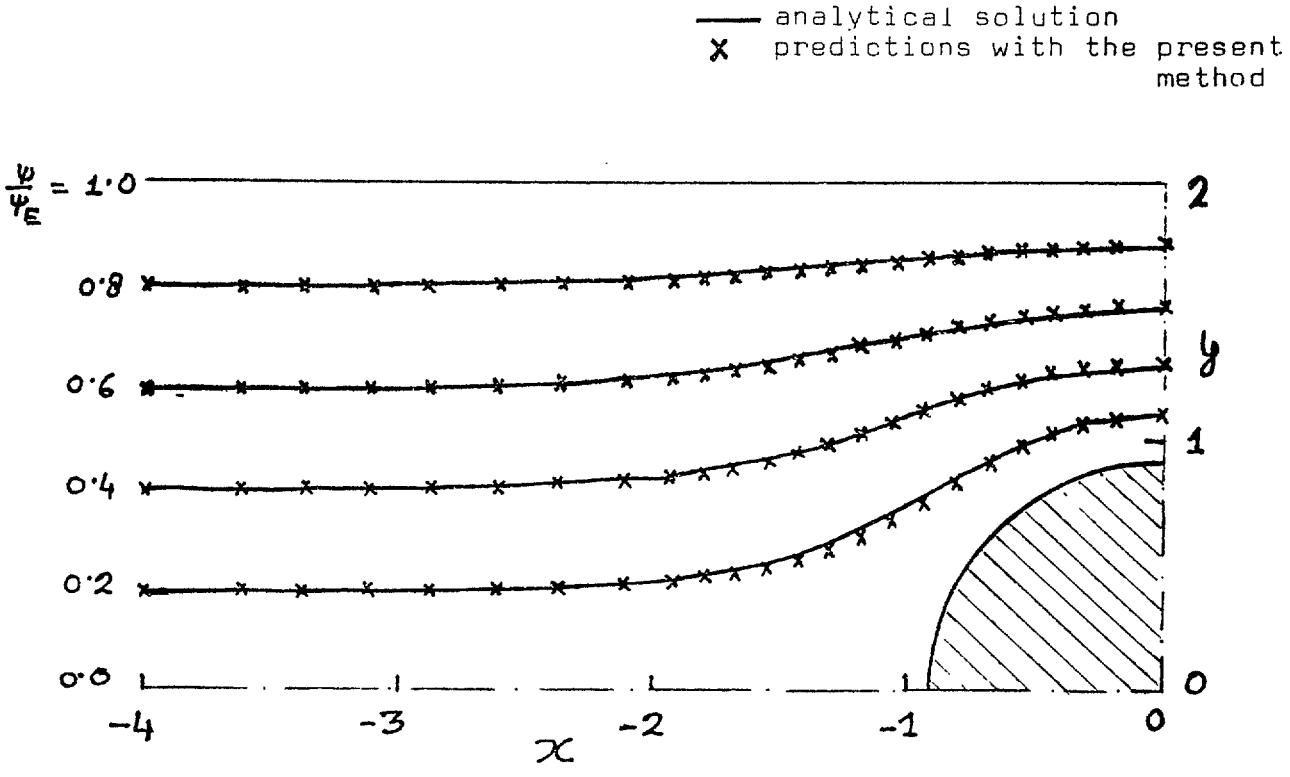

FIG. 8. Comparison between prediction and analytical solution of the streamlines.

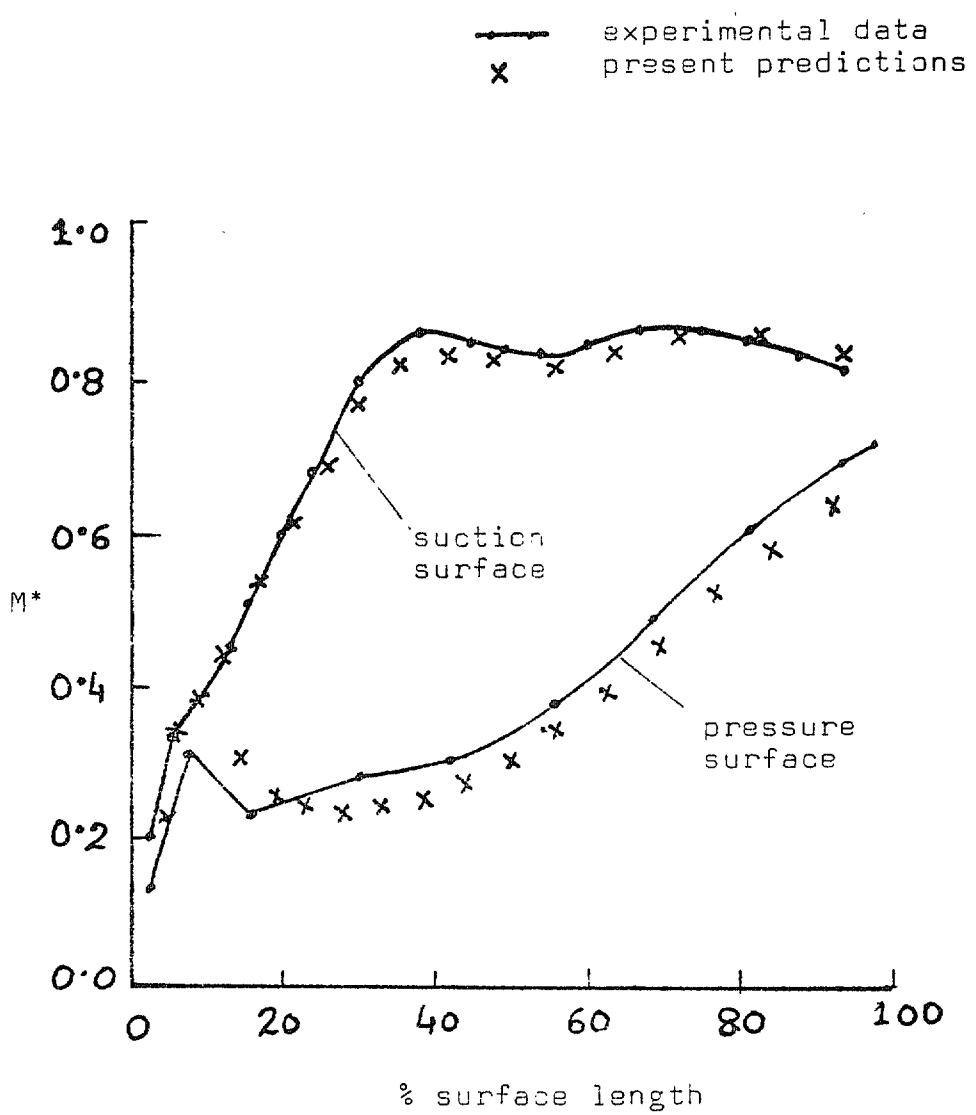

FIG. 9. Comparison of predicted surface velocities with experimental data; NASA turbine stator cascade.

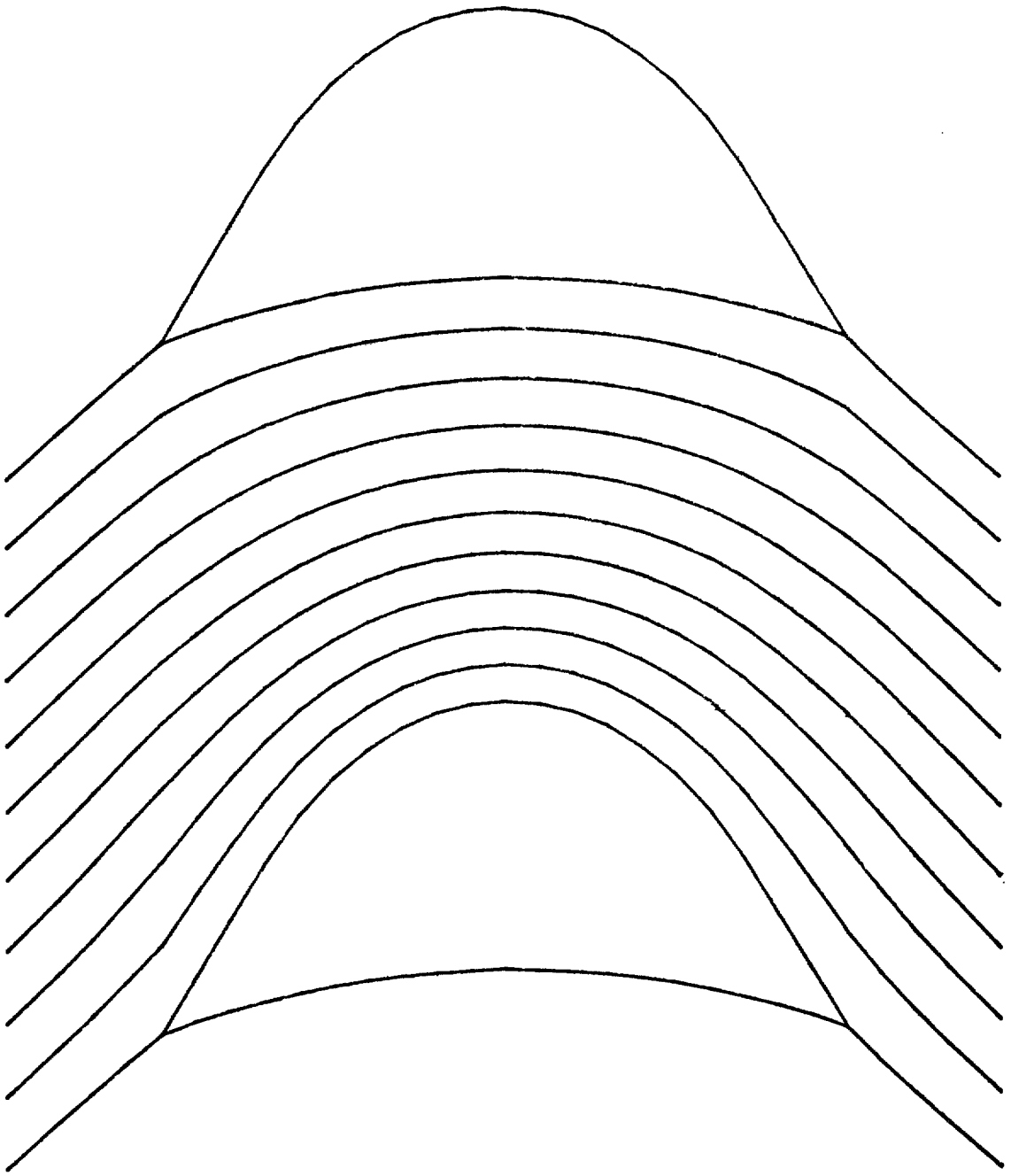

FIG. 10. Computed streamlines; Hobson's first impulse cascade.

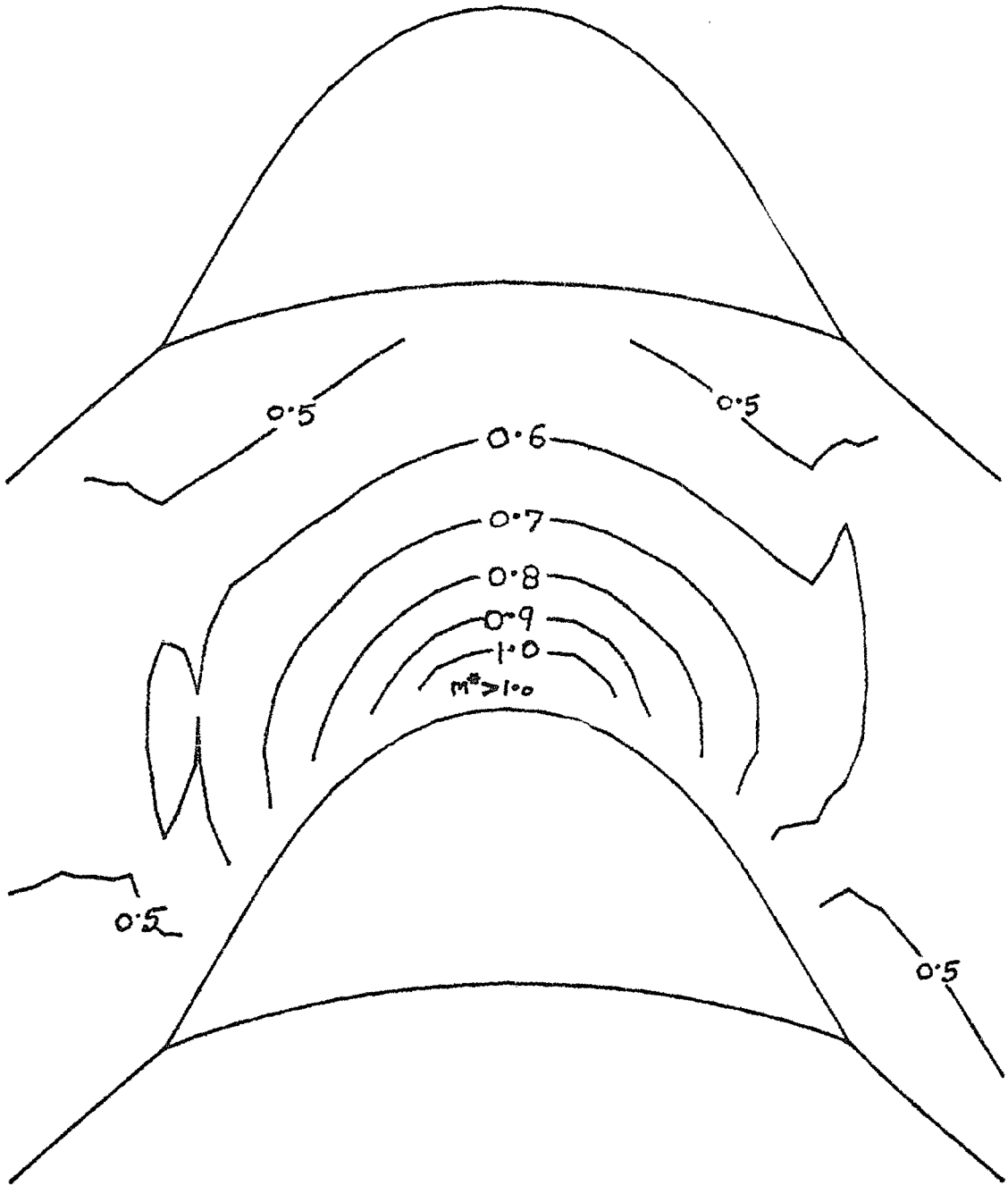

FIG. 11. Critical-Mach-Number contours; Hobson's first impulse cascade.

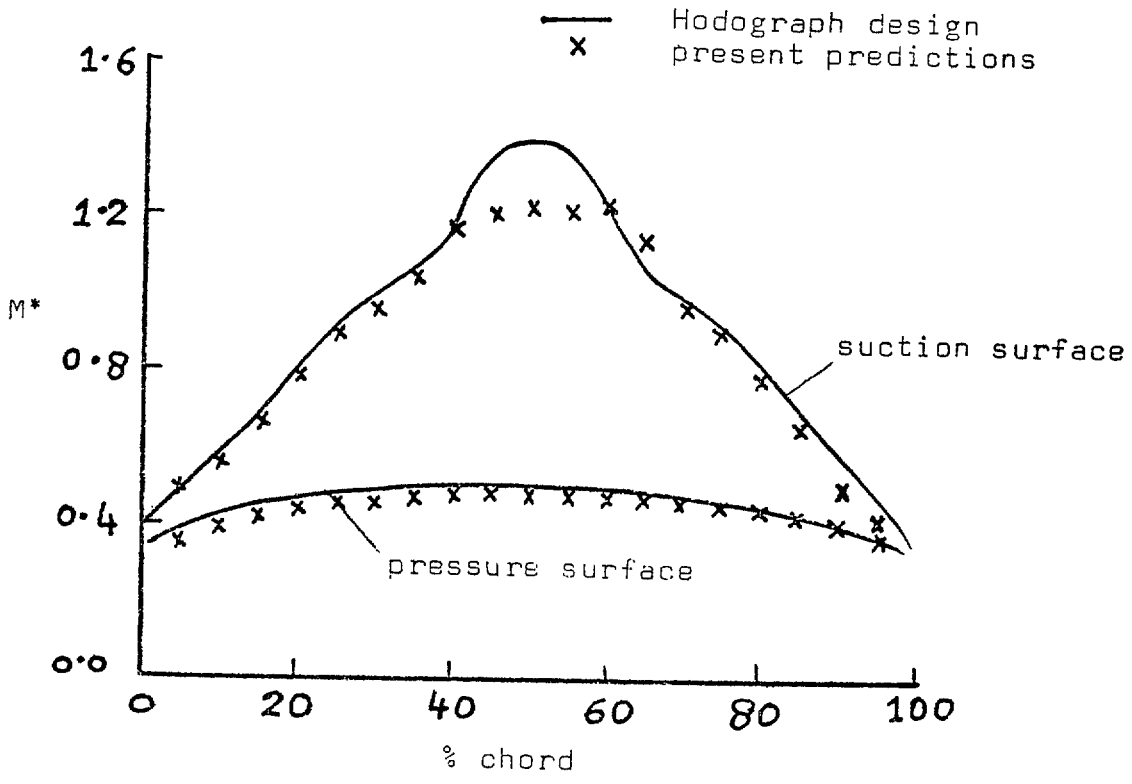

FIG. 12. Distribution of surface velocities; Hobson's first impulse cascade.

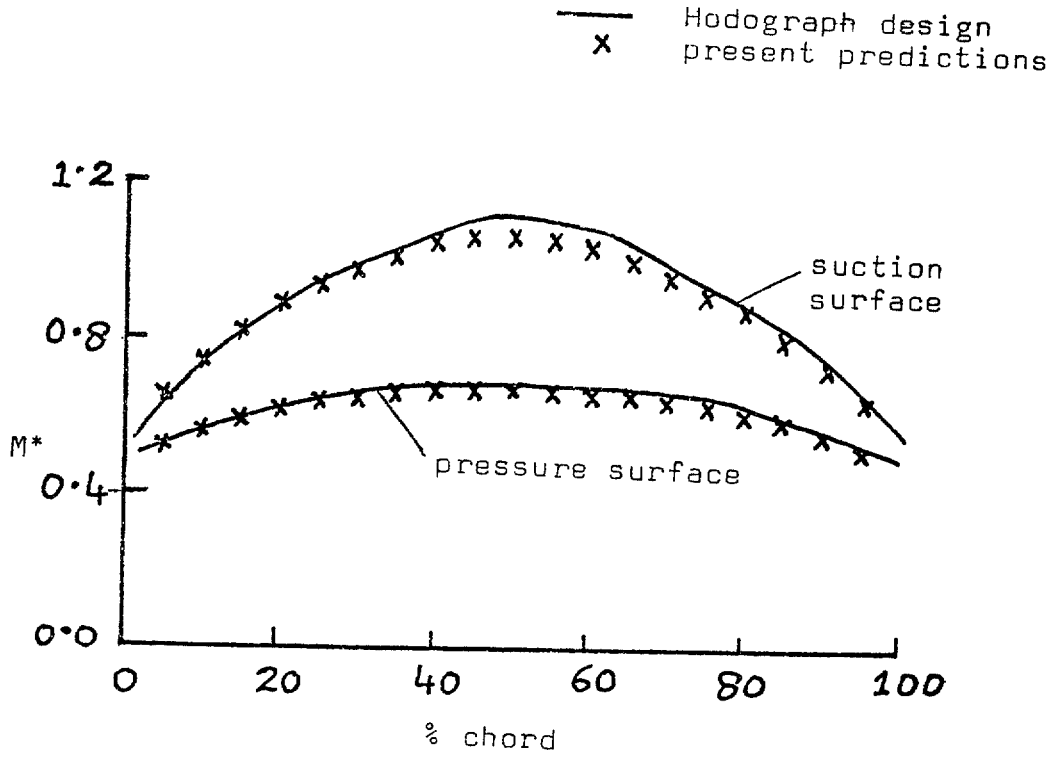

FIG. 13. Distribution of surface velocities; Hobson's second impulse cascade.

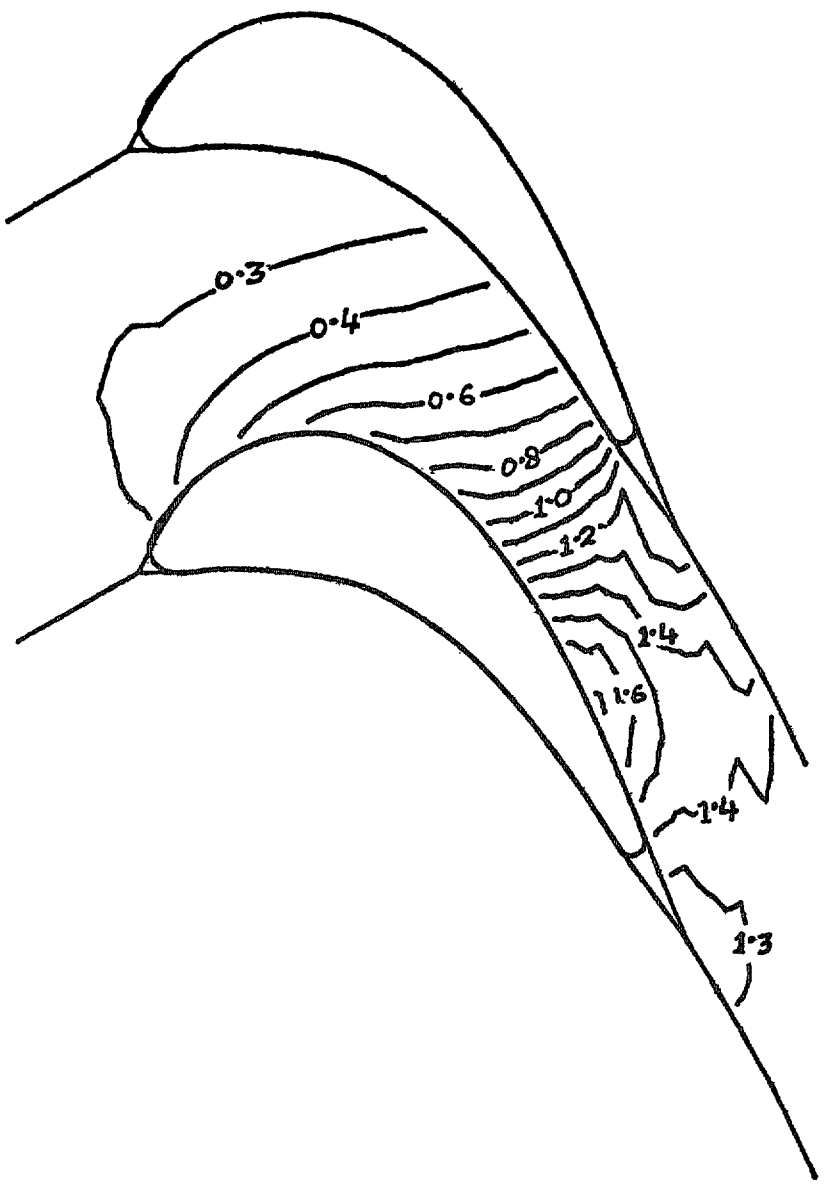

FIG. 14. Mach-number contours; VKI gas turbine cascade. (Outlet Mach No. = 1·31).

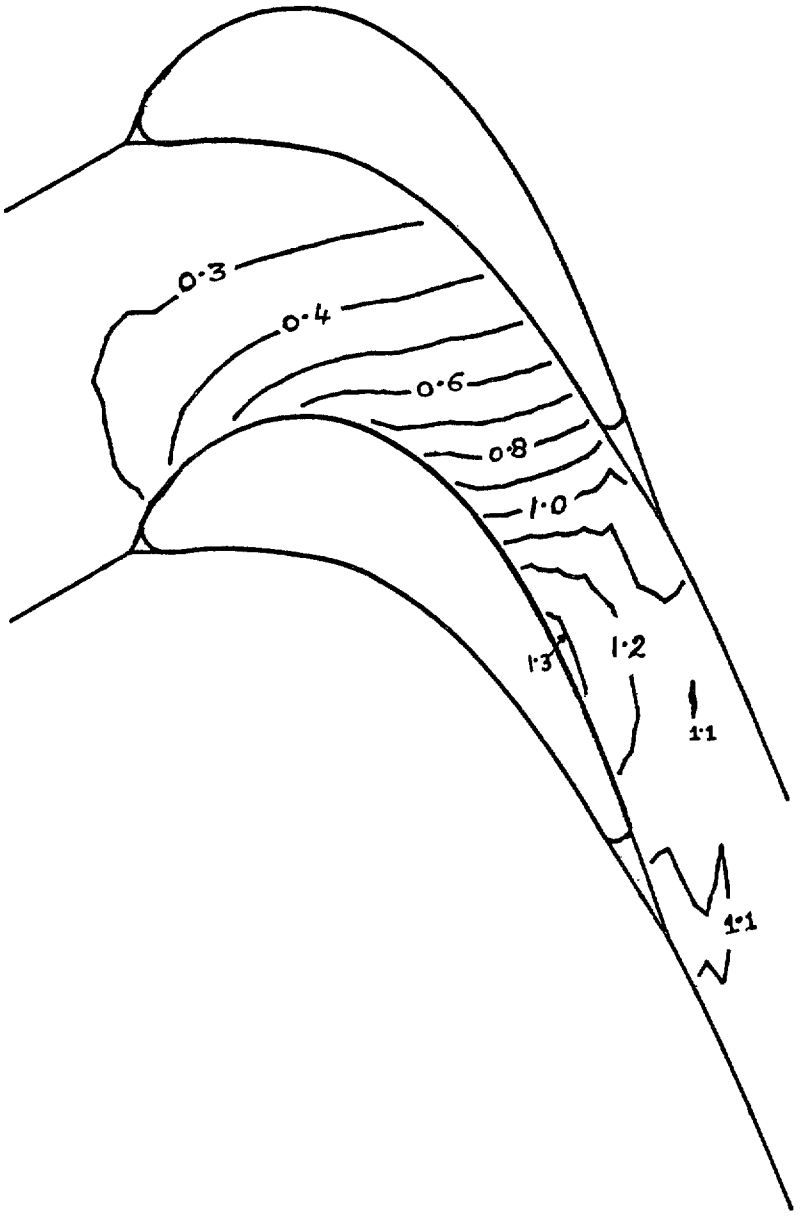

FIG. 15. Mach-number contours; VKI gas turbine cascade. (Outlet Mach No. = 1·11).

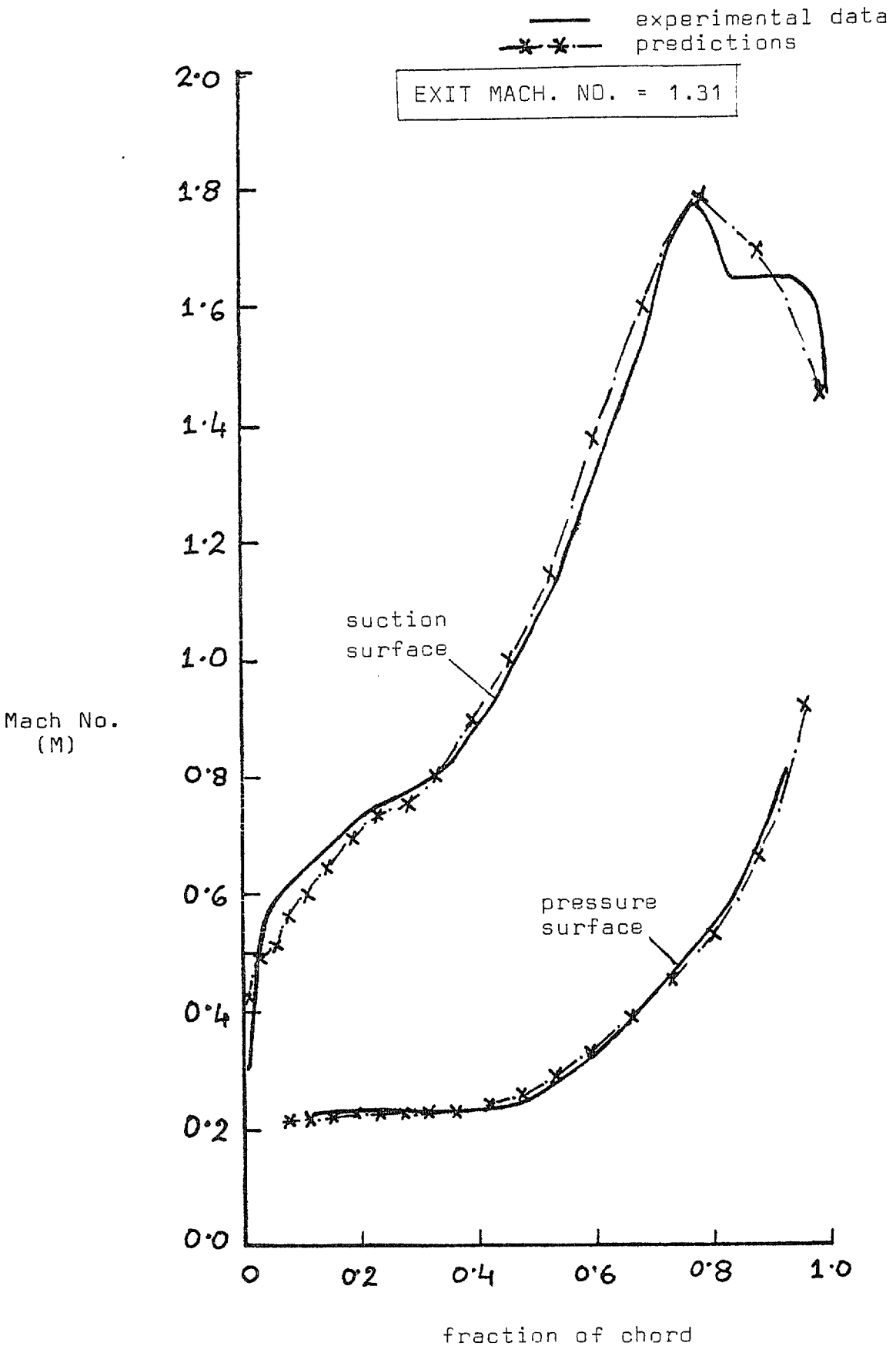

FIG. 16. Distribution of surface Mach numbers; VKI gas turbine cascade.

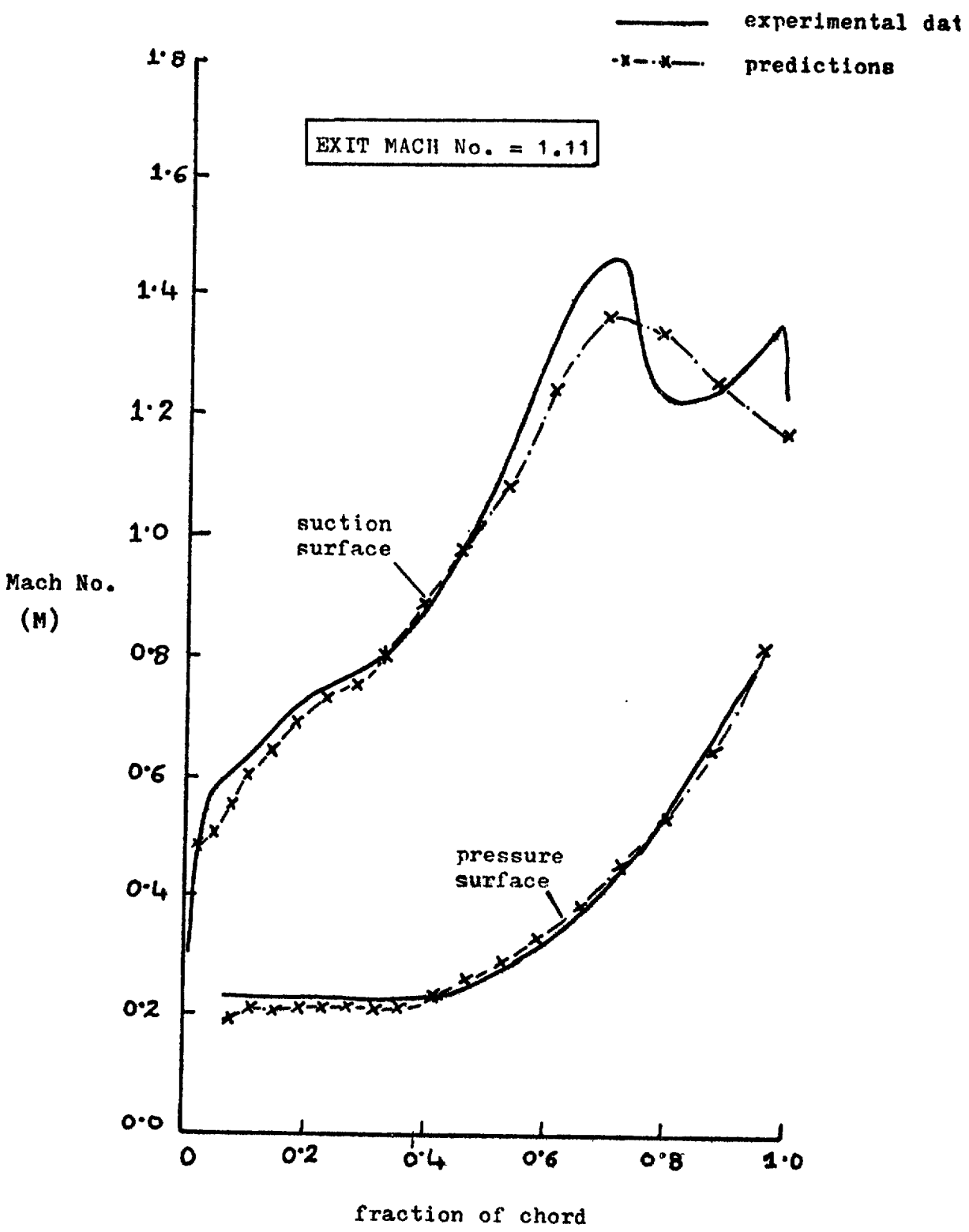

FIG. 17. Distribution of surface Mach numbers; VKI gas turbine cascade.

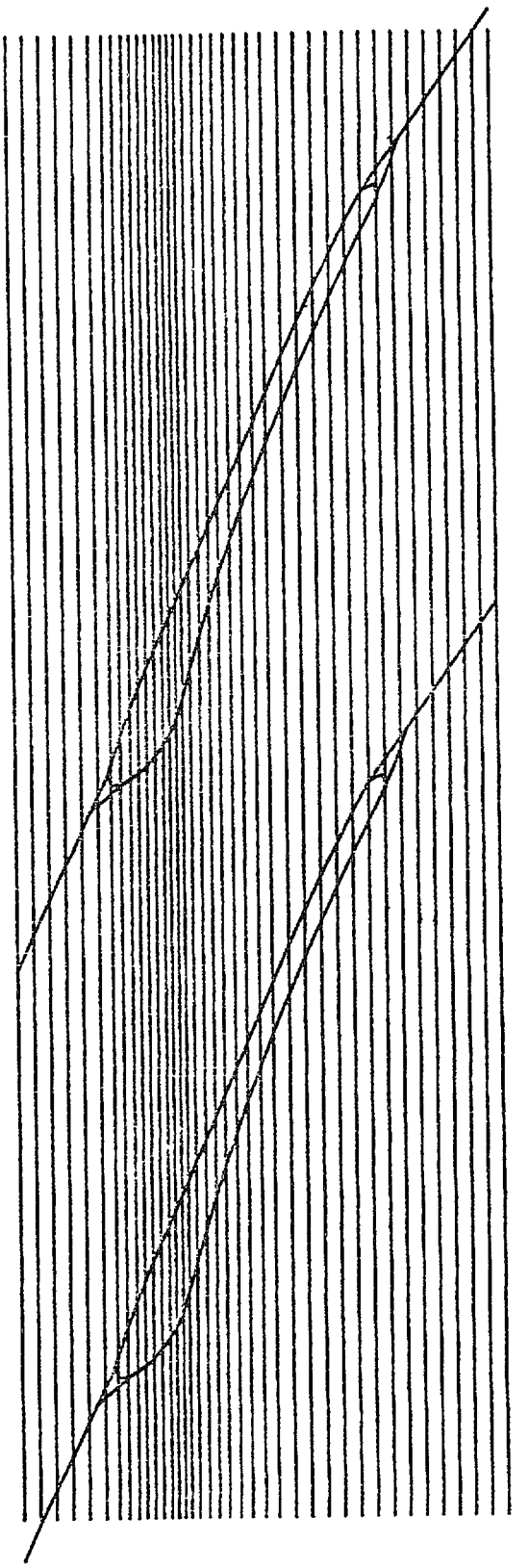

FIG. 18. Pitchwise grid lines; VKI steam turbine cascade. (Outlet Mach No. = 1·80).

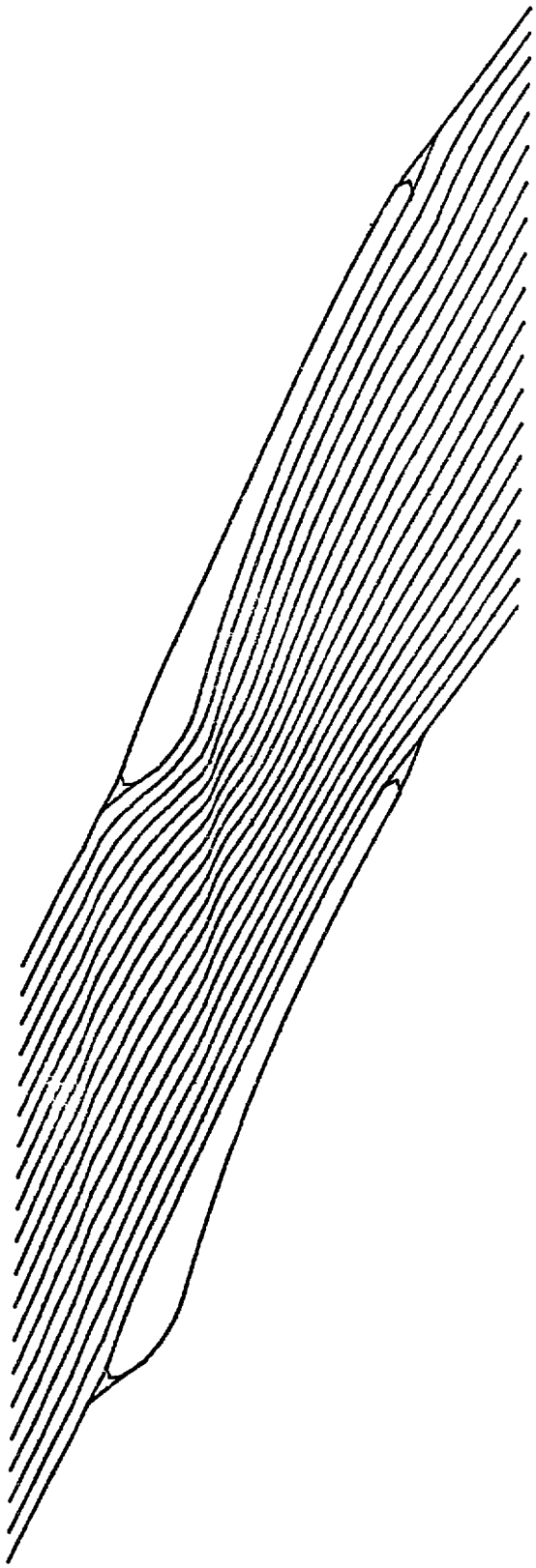

FIG. 19. Computed streamlines; VKI steam turbine cascade. (Outlet Mach No. = 1·80).

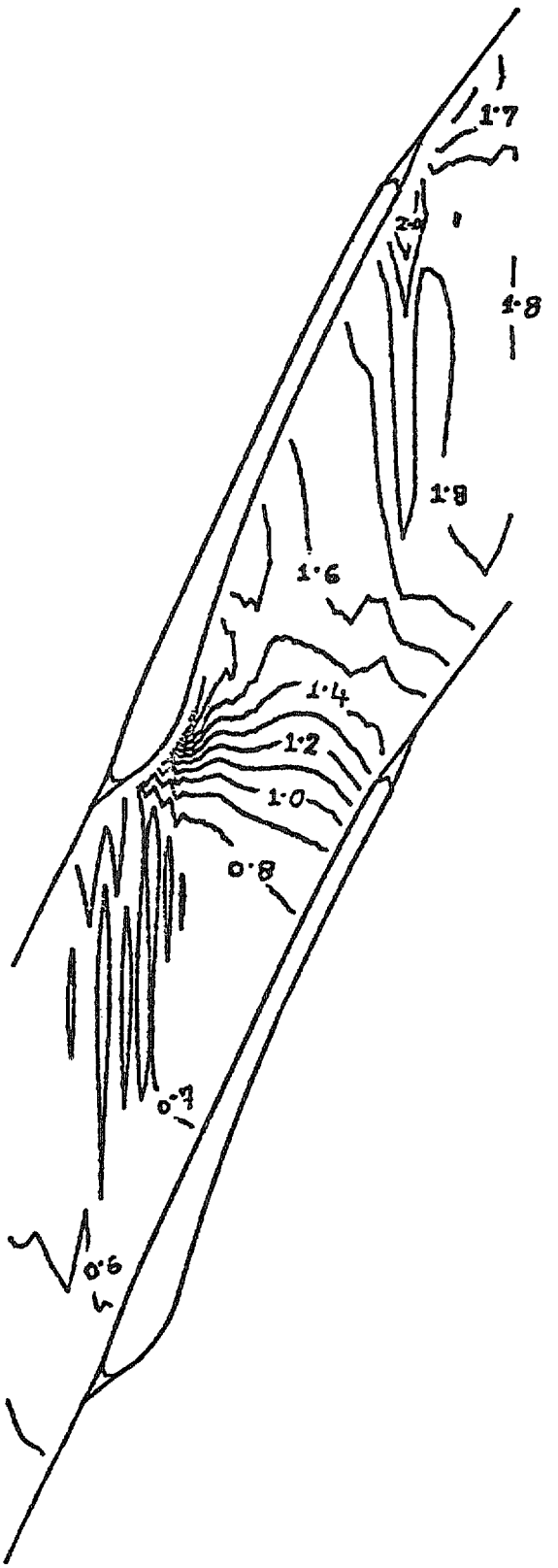

FIG. 20. Mach-number contours; VKI steam turbine cascade. (Outlet Mach No. = 1·80).

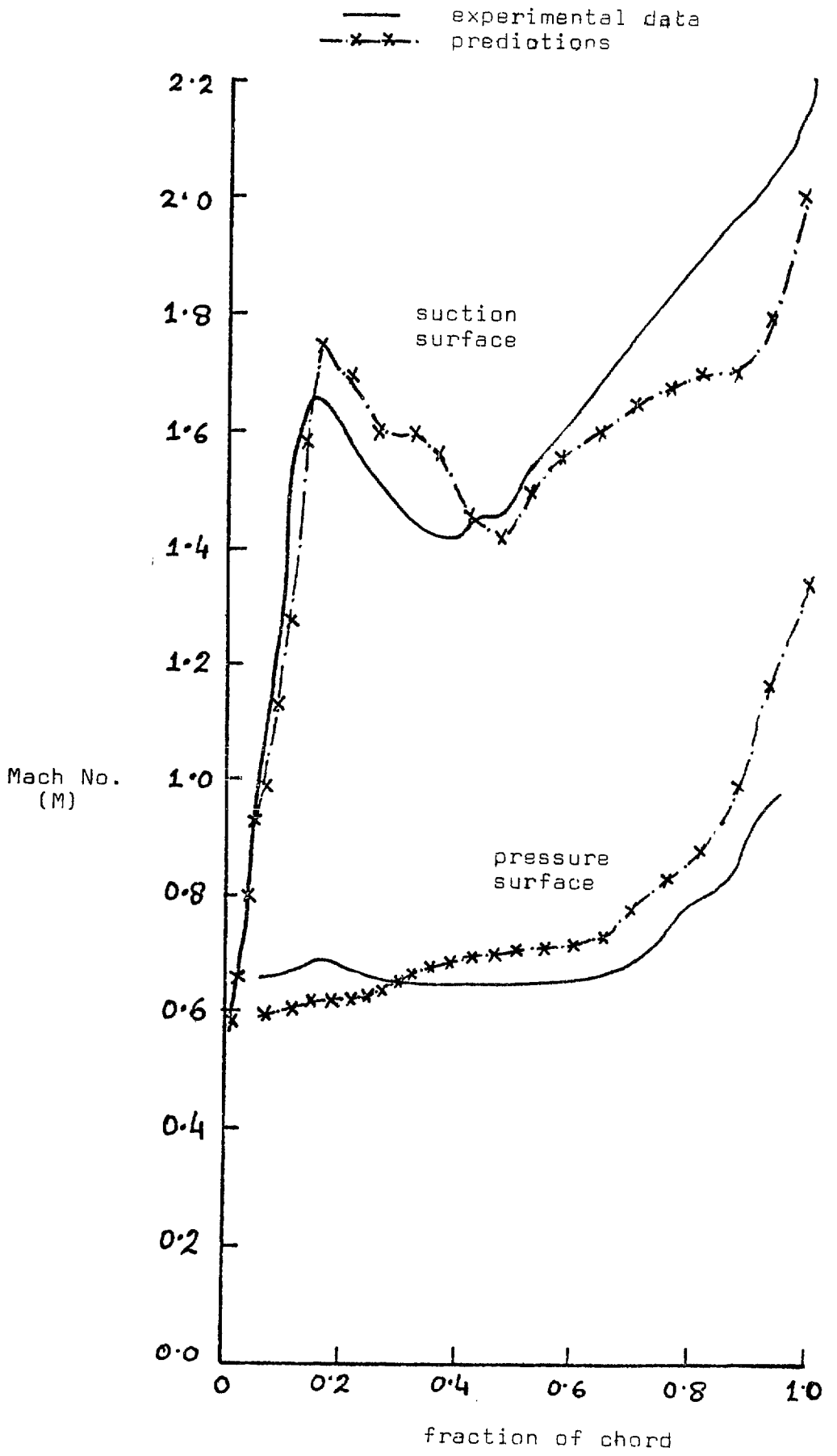

FIG. 21. Distribution of surface Mach numbers; VKI steam turbine cascade.

HER MAJESTY'S STATIONERY OFFICE

Government Bookshops

49 High Holborn, London WC1V 6HB
13a Castle Street, Edinburgh EH2 3AR
41 The Hayes, Cardiff CF1 1JW
Brazennose Street, Manchester M60 8AS
Southey House, Wine Street, Bristol BS1 2BQ
258 Broad Street, Birmingham B1 2HE
80 Chichester Street, Belfast BT1 4JY

Government Publications are also available through booksellers

ISBN 0 11 470978 5